Mathematical Biosciences and Engineering

MBE, 16(5): 4873–4884.
DOI: 10.3934/mbe.2019245
Received: 20 December 2018
Accepted: 06 May 2019
Published: 29 May 2019

http://www.aimspress.com/journal/MBE

Research article

High-frequency temperature pulse-response behavior through a porous nanocomposite scaffold for measuring the uptake of biological fluids

Christophe Minetti[1], Carlo S. Iorio[1] and Hatim Machrafi[1,2,*]

[1] Service Chimie-Physique, Université libre de Bruxelles, Brussels, Belgium
[2] GIGA-In Silico Medicine, Université de Liège, Liège, Belgium

*** Correspondence:** Email: h.machrafi@ulb.ac.be.

Abstract: The measurement of biological fluid uptake into a scaffold sensor has been modeled by measuring the response of induced high-frequency temperature pulses. For this, a heat transport equation is used, developed from Extended Thermodynamics, also equivalent to Cattaneo's equation, as well as an effective thermal conductivity. The effective thermal conductivity is experimentally validated against data measurements of a carbon nanotube porous nanocomposite, embedded with silica nanoparticles. This nanocomposite serves also as the case study for the scaffold sensor. The uptake of the biological fluid in this scaffold sensor is equivalent to a change in the effective thermal conductivity, monitored by an increase of the interstitial volume fraction. By imposing a high-frequency temperature oscillation, the temperature response at the other end of the porous medium is calculated. Depending on the ratio of the relaxation time and the thermal diffusion time, the temperature response can be of oscillatory nature or of an exponential growth to an asymptotic limit. It is observed that an observed phase lag in the temperature response indicates a change in the effective thermal conductivity and thus is a criterion denoting the amount of uptake.

Keywords: high-frequency pulse-response; extended thermodynamics; self-assembled porous nanocomposite; biological fluid uptake; relaxation time

1. Introduction

In the medical field, it is of interest in measuring the uptake of certain fluids that are indicators of corresponding complications. One way to do so is placing a scaffold on the spot where those biological fluids may be present. Such scaffolds are typically of porous nature and may contain also

nanoparticles for structure reinforcement. The porous scaffolds have their own properties depending on the porosity and nanoparticle content, besides the scaffold itself. The properties in question may be of thermal, electrical or mass diffusional nature. When the scaffold absorps some biological fluid, it is natural to say that this changes the aforementioned properties. We are interested here by the thermal properties. By introducing thermal pulses of high frequency on one side of such a porous scaffold and measuring the response on the other side, one is able to deduce from the response whether some biological fluid has been taken up. Since many factors may play a role in such an analysis, modelling can provide for useful tools that can be used to compose such sensors. It is well known that Fourier's law is not valid for high pulse responses. For information from biosensors in case of continuous monitoring, other models should be proposed. We propose a model that can be used for such purposes concerning a porous medium, in which nanoparticles are dispersed. Besides the model representing the evolution of the heat flux and the temperature, we need also a model that describes how the thermal diffusion through the porous medium is affected by the biological fluid uptake. We propose to do this by using an effective thermal conductivity, adapted from [1,2]. This effective thermal conductivity is valid at the condition that the thermal conductivity of the scaffold is much higher than that of air and the nanoparticles. This is justified since we use as scaffold a medium self-assembled from carbon nanotubes (CNT), wherein silica (SiO_2) nanoparticles are embedded for reinforcement and alignment of the CNTs for a better conductivity [3]. The fabrication process and characterisation of this scaffold has been presented in previous work [3]. Since it is important to use a correct effective thermal conductivity, we validate this against experiments of self-assembled CNT-SiO_2 porous nanocomposites.

The self-assembly procedure is applied in various forms in many fields [4–12]. The one against which we validate the effective thermal conductivity is explained in details in [3]. Essentially it resumes to the following. By using drop-by-drop evaporation of aqueous solutions of CNT and SiO_2, we deposit multiple self-assembled layers of CNTs and SiO_2 on a substrate. The obtained dry residu is a porous structure that, depending on the initial parametric conditions, can have different properties. As mentioned before, the focus is on the thermal conductivity. The porosity of the scaffolds and the volume fraction of the nanoparticles are also determined from those experiments. The data are imported in our model, leading to a heat flux and temperature evolution depending on the porosity and volume fraction of the scaffold medium. Since in the model used for the effective thermal conductivity, the thermal conductivity of air and the nanoparticles are considered to be negligible with respect to that of CNT, it is solely dependent on the porosity and nanoparticles. The biological fluid that is being taken up in the scaffold has also a thermal conductivity negligible to that of CNT, so that it can be treated on the same level as the nanoparticles. So, an uptake of the biological fluid is equivalent to an increase of the volume fraction of nanoparticles in the scaffold. The idea is to impose high-frequency temperature pulses and calculating their response at the other side. By varying the volume fraction, one is able to calculate the response to a fixed heat pulse, being indicative of measuring biological fluid intake. Our model is developed in section 2 and the experimental data needed for the model in section 3. Section 4 discusses the results and section 5 concludes.

2. Theory

A previously developed model from Extended Thermodynamics proposes constitutive equations for the thermal transport taking into account non-localities [13]. In case the system size is much larger than the mean free path of the thermal carriers, a one-dimensional version of the constitutive equation for the heat flux, q can be given by

$$\tau_r \partial_t q + q = -\lambda_{eff} \partial_x T \tag{1}$$

where τ_r, t, x, λ_{eff} and T are the relaxation time of the heat flux, the time and space coordinates, the effective thermal conductivity and the temperature, respectively. The one-dimensional balance equation for energy is

$$\rho c_p \partial_t T = -\partial_x q \tag{2}$$

with ρ and c_p the density and heat capacity, respectively. In (1)–(2), the thermal conductivity for a porous structure is given by [2,14].

$$\lambda_p = \lambda_0 \frac{2-2\varepsilon}{2+\varepsilon}. \tag{3}$$

where λ_0 denotes the thermal conductivity for the bulk material, and ε stands for its porosity. If nanoparticles are homogeneously inserted in such a porous matrix (for instance, by depositing a droplet containing a mixture of CNTs and nanoparticles) then, for the thermal conductivity, (3) should be adapted:

$$\lambda_{eff} = \lambda_p \frac{2-2\varphi}{2+\varphi} = \lambda_0 \frac{2-2\varepsilon}{2+\varepsilon} \frac{2-2\varphi}{2+\varphi}, \tag{4}$$

where φ is the volume fraction of the nanoparticles. Note that in (3)–(4), simplifications are introduced with respect to [2,14], because of the much higher thermal conductivity of CNT with respect to air and even with respect to the silica nanoparticles. The difference in the phonon relaxation times of CNTs, SiO_2 and biological fluids being less important here than the difference in thermal conductivity, we will assume that its dependence on the volume fraction is negligible, so that:

$$\tau_r = \tau_{r0} \tag{5}$$

with τ_{r0} the relaxation time of the bulk material. For computational purposes, our model is rendered dimensionless. We choose for the time scale τ_{r0}, for the spatial scale the system's size δ, for the heat flux $\frac{\lambda_0 \Delta T}{\delta}$, and for the temperature $T \to \frac{T-T_0}{\Delta T}$. Herein, $\Delta T = T_i - T_0$, where the subscripts i and 0 indicate a maximum and minimum temperature to which the material is exposed to. In case there is an imposed oscillatory boundary temperature, T_i would stand for the peak maximum temperature and T_0 for the peak minimum temperature, which is also chosen to be the initial one. This gives for heat transport, writing the same symbols for the dimensionless quantities, the following set of equations

$$\partial_t q + q = -\frac{2-2\varepsilon}{2+\varepsilon} \frac{2-2\varphi}{2+\varphi} \partial_x T \tag{6}$$

$$\partial_t T = -\alpha_{th} \partial_x q \tag{7}$$

with $\alpha_{th} = \frac{\tau_{r0}}{\tau_{th}}$, the thermal diffusion characteristic time being defined by $\tau_{th} = \frac{\delta^2}{\kappa_{th}}$, with $\kappa_{th} = \frac{\lambda_0}{\rho c_p}$ the thermal diffusivity. The boundary conditions are given by a zero-heat-flux condition, i.e. $q = 0$ (which means a zero-temperature-gradient in virtue of (1)) at the measuring point ($x = 0$) and an imposed oscillatory temperature at the other side ($x = 1$), with frequency $\omega = P/\tau_{r0}$, where P is a value determining the periodicity of the oscillations with respect to the relaxation time. The dimensionless versions are

$$\partial_x T|_{x=0} = 0 \tag{8}$$

$$T|_{x=1} = \frac{1}{2}(1 - \cos(2P\pi t)) \tag{9}$$

For convenience, the form of boundary condition (9) has been chosen as such to assure a positive value of T for all t.

3. Experimental

This section presents experimental data, which will serve in section 4 to validate the model for the effective thermal conductivity as a function of the porosity for a certain determined fixed volume fraction of dispersed nanoparticles.

3.1. Experimental procedure for the scaffold formation

The process of the drop-deposition experiment is described by the deposition of droplets that contain nanomaterial, letting them evaporate at room temperature and ambient humidity (60% humidity) for seven hours. The duration of the process was needed not so much to evaporate the droplets as such, but rather to evacuate the water that is held back in the pores due to the capillary pressure, since the deposited nanomaterial creates a nano-porous network. The droplets, used for the depositions, contain a mixture of CNTs and SiO_2 nanoparticles. The 3 g/L aqueous 5 nm multi-walled CNT dispersion has been supplied by Nanocyl and the 0.3 g/L aqueous 175 nm SiO_2 has been supplied by Bangs-Laboratories. The CNT solutions are kept in homogeneous dispersion by the presence of anionic surfactants, which guarantee a long-lasting stable homogeneous aqueous dispersion of the CNTs. As for the SiO_2 solutions, they are found to remain in a stable homogeneous aqueous dispersion due to Si-OH surface groups. As recommended by the fabricants, the aqueous solutions are sonicated before depositing the droplets. The position of the droplet is controlled by a motor with a precision of 0.01 mm. Each droplet is deposited by a syringe on a spot that is delimited by a groove, which creates pinning conditions. This results into 40 μL droplets with a diameter of 12 mm. The drop deposition setup has been developed in the lab (Physical Chemistry Group) and is made of a bi-dimensional translation stage (Moons STM17S-1AE) and a home-made double syringe pump using the same motorized stages. The software drives automatically the setup and acquires images of the drop after each deposition (camera JAI BM-500GE) to control the volume of the drop. As soon as the droplets are deposited, the start to evaporate, which induces convectional instabilities. The CNTs and SiO_2 nanoparticles move along the flow lines. After the fluid has evaporated, the nanoparticles and CNTs settle on the substrate, forming a porous nanostructure.

3.2. Material properties

The porosity of the matrix is defined as

$$\varepsilon = \frac{V_p}{V_t - V_{np}} = 1 - \frac{V_m}{V_t - V_{np}} = 1 - \frac{(N_d+1)\frac{C_m V_d}{\rho_m}}{\pi r_m^2 \delta_m - N_d \frac{C_{np} V_d}{\rho_{np}}} \tag{10}$$

where V_p, V_m and V_{np} are the pore volume (air in our case), the volume occupied by the matrix (CNT) and the volume occupied by the nanoparticles (SiO_2), respectively (note that the total volume is $V_t = V_p + V_m + V_{np}$). Moreover, C_m is the matrix material concentration in the deposited droplet ($C_m = 3$ g/L), C_{np} is the silica concentration in the deposited droplet ($C_{np} = 0.3$ g/L), ρ_m the CNT "tap" density ($\rho_m = 1.6$ kg/L), ρ_{np} the silica density ($\rho_{np} = 2.65$ kg/L) and V_d the volume of each deposited droplet ($V_d = 40$ µL). The term $(N_d + 1)$ in (10) stands for the fact that before depositing the CNT-SiO_2 mixtures, one layer of pure CNT is deposited [3]. The calculated porosity presents an error of less than 0.5% and is presented in Table 1 as a function of the number of deposited droplets. Furthermore, in (10), δ_m and r_m are the thickness of the deposited material and the radius, respectively. The radius is measured to be $r_m = 6$ mm and δ_m is measured by means of a confocal probe [3] and also given in Table 1.

Table 1. Calculated ε and δ_m as a function of N_d.

N_d	1	2	3	4	5	6	7
ε	0.83	0.83	0.85	0.84	0.82	0.80	0.81
δ_m [µm]	8.0	11.9	18.1	20.9	22.3	24.0	28.0

The volume fraction of the nanoparticles used in the aforementioned material can be calculated via

$$\varphi = \frac{C_{np}}{\frac{\rho_{np}}{\rho_m} C_m + C_{np}} \tag{11}$$

which gives $\varphi = 0.057$.

Since it is quite difficult to find the exact values for λ_0, they will be taken from experimental findings from [3] of pure CNT depositions. It is found that for a pure monolayer nanoporous CNT, $\lambda_p = 0.88$ kW/Km. With a porosity (calculated from data from [3], with a droplet volume of 45 µL and using Eq (10) with $N_d = 2$ and $\delta_m = 20$ µm) of $\varepsilon = 0.85$, we find easily from Eq (3) as approximation that $\lambda_0 = 8.4$ kW/Km (which is, taking into account experimental uncertainty, not far from the 6600 W/Km found in the literature [14].

4. Results and discussion

4.1. Experimental data

The deposited nanostructures, for several number of deposited droplets (see Table 1), are measured for their effective thermal conductivity, λ_{exp}. The results are presented in Table 2.

Table 2. Measured thermal conductivities.

N_d	1	2	3	4	5	6	7
ε	0.83	0.83	0.85	0.84	0.82	0.80	0.81
$\lambda_{\parallel}$ [kW/Km]	0.88	0.89	0.93	0.89	0.96	1.00	0.98

Table 2 shows that, in overall, the thermal conductivities increase, with an overall decreasing porosity, which suggests indeed that a denser structure is obtained, which can be explained by a better alignment of CNTs. In general, a composite structure that becomes denser than the CNT structure, would lead to a relative increase of the thermal conductivity with respect to its initial value. As for the alignment of the CNTs, this is confirmed by SEM images in [3] and is not the subject of the present work. In general, as the degree of alignment of CNTs is higher, the thermal conductivity should increase in the axial direction of the nanotubes.

4.2. Validation

For practical purposes (applications as biosensors, batteries, rather than insulators, semi-conductors), the interest lies more into the conductivities in the longitudinal direction of the CNTs. For a preferred substrate direction, even though the CNTs are not perfectly aligned , the longitudinal axis of the majority of the CNTs will still be in that preferred direction. The experimental data used for this purpose are taken from section 4.1. Nevertheless, for the sake of completeness, important details are represented next. With our model, the effective thermal conductivities are calculated from the model in section 2 and compared to the experimental values. The results are presented in Figure 1.

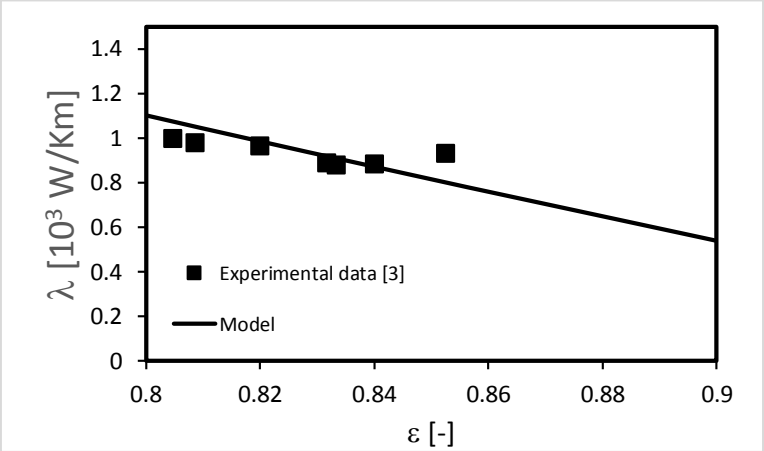

Figure 1. Effective thermal conductivity of the porous SiO_2-CNT nanocomposite as a function of porosity. Squares are the experimental results from Table 2 and the lines represent our model.

Figure 1 shows a good agreement between the model and the experiments, showing that a lower porosity corresponds to higher thermal conductivities. The results confirm the validity of the model for the effective thermal conductivities for the purposes of this work.

4.3. High frequency response for thermal transport

In the expression of the thermal characteristic time, the thermal conductivity is that of the bulk material (i.e. $\lambda_0 = 6600$ W/(Km)), whilst the density and heat capacity are those of the porous medium. Taking a volume-fraction-based weighted average (the densities of CNT and air are 1600 and 1.2 kg/m^3, respectively, whilst the heat capacities of CNT and air are 620 [16] and 1005 J/(kgK) , respectively), noting that the porosity is defined on volume basis and that ε=O(0.85), we find $\rho = 241$ kg/m^3 and $c_p = 947$ J/(kgK). The relaxation time for a CNT-SiO_2 system is given in [17] to be $\tau_{r0} = 85$ ps. Taking for the thickness a value of the same order of magnitude as Table 1, let us say $\delta = O(10)$ μm, we find a thermal characteristic time of $\tau_{th} = 31$ ns. This gives $\alpha_{th} \approx 2.5 * 10^{-2}$. For this value, our model is used for the calculations by means of the programme Mathematica. Figure 2 shows a 3D example for $\varphi = 0.057$.

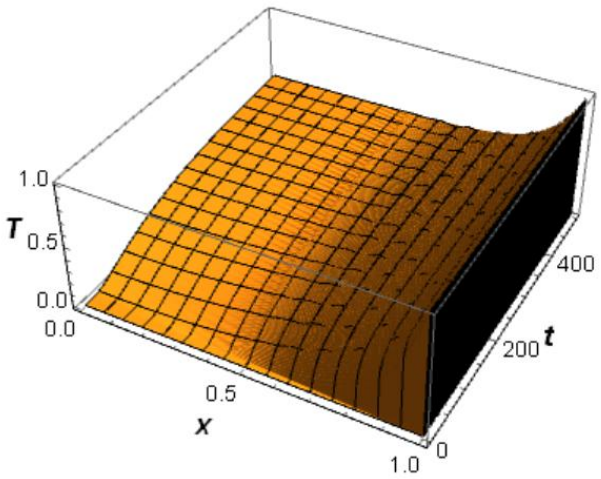

Figure 2. Temperature T across the one-dimensional porous nanocomposite layer x as a function of time t for $\alpha_{th} \approx 2.5 * 10^{-2}$, $\varphi = 0.057$ and $P = 0.5$.

Figure 2 shows that the oscillations at $x = 1$ (not clearly visible, because the period of the temperature oscillations is equivalent to 2t on a scale of 400t in the Figure) are quickly damped. This is due to the relaxation time being much smaller than the thermal diffusion time. Furthermore, this damping also results into a delayed response, due to the presence of a relaxation time in se. The temperature at the other side increases to a value equal to the mean value of the oscillatory temperature, i.e. $T = 0.5$. In order to visualize this more, it is more convenient to plot the response temperature (i.e. T at $x = 0$) as a function of time. We do this for four values of $\varphi = 0.057$, 0.1, 0.2 and 0.5. The results are presented in Figure 3.

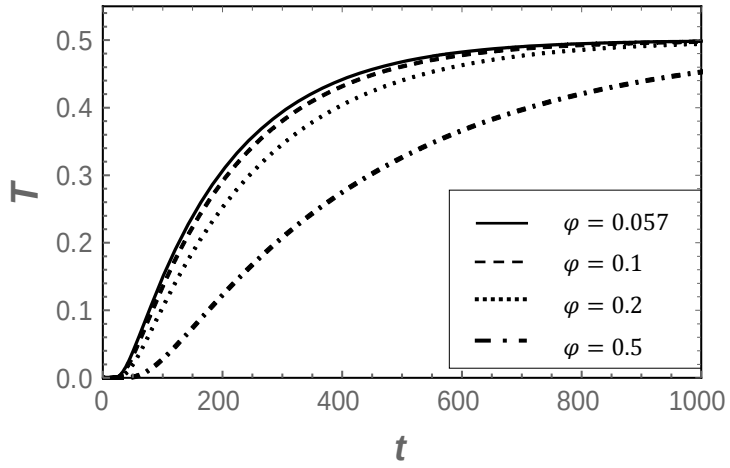

Figure 3. Temperature T at $x = 0$ as a function of time t for $\alpha_{th} \approx 2.5 * 10^{-2}$ and different values of the volume fraction φ (the volume fraction of the biological fluid uptake is given by $\varphi_b = \varphi - 0.057$).

Note that the volume fraction for the biological uptake is given by $\varphi_b = \varphi - 0.057$. So, $\varphi = 0.057$ is the reference state (the value corresponding to the silica nanoparticles), where no biological fluid has been taken up yet. We can see indeed that no oscillations are present (fully damped) and that the uptake of the biological fluid ($\varphi > 0.057$) results into a decrease of the temperature response, which is attributed to the decrease in the effective thermal conductivity. A way to measure the evolution of the uptake of biological fluid would be following the gradient of the temperature evolution, indicative for the time needed to attain the final value of $T = 0.5$. For illustrative purposes, we perform the same calculations also for $\delta = O(3.5)$, $\delta = O(1.5)$ and $\delta = O(1)$ μm, so that $\alpha_{th} = O(0.2)$, $\alpha_{th} = O(1)$ and $\alpha_{th} = O(2.5)$, respectively. These results are presented in Figures 4 to 6, respectively.

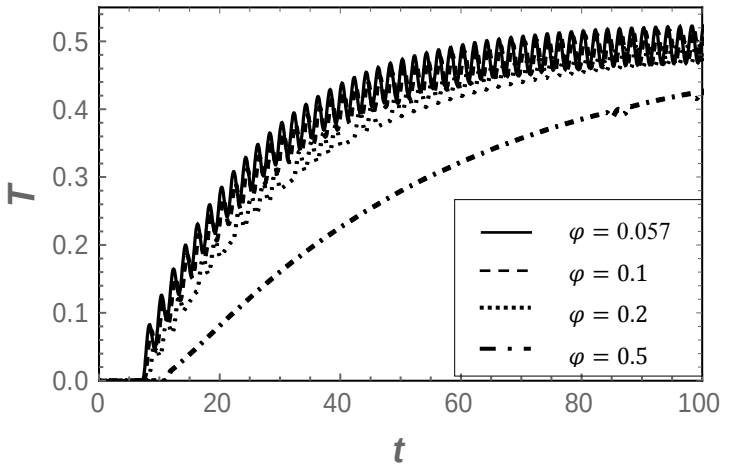

Figure 4. Temperature T at $x = 0$ as a function of time t for $\alpha_{th} = 0.2$ and different values of the volume fraction φ (the volume fraction of the biological fluid uptake is given by $\varphi_b = \varphi - 0.057$).

Figure 4 shows that a higher value of α_{th} (the thermal diffusion time becomes smaller than in the previous case, which could be due to another material or another thickness of the same material) results into a small "left-over" of the imposed oscillations, but keeping approximately the same incremental tendency.

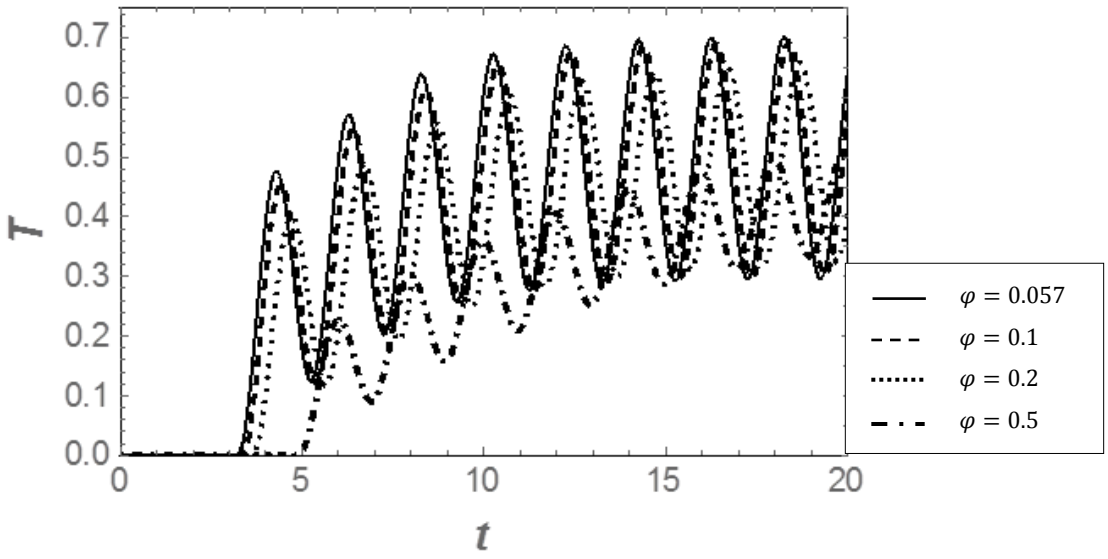

Figure 5. Temperature T at $x = 0$ as a function of time t for $\alpha_{th} = 1$ and different values of the volume fraction φ (the volume fraction of the biological fluid uptake is given by $\varphi_b = \varphi - 0.057$).

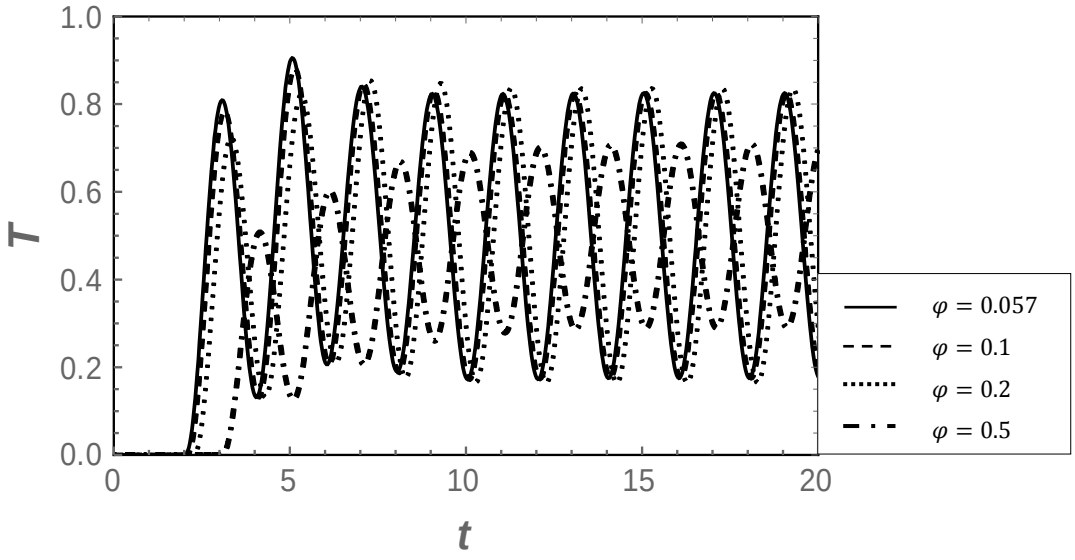

Figure 6. Temperature T at $x = 0$ as a function of time t for $\alpha_{th} = 2.5$ and different values of the volume fraction φ (the volume fraction of the biological fluid uptake is given by $\varphi_b = \varphi - 0.057$).

Figure 5 shows that, for a relaxation time of the order of magnitude of a thermal diffusion time, the incremental behaviour is only slightly visible, but rather the oscillatory behaviour of the temperature response becomes more important. As such, for higher values of φ (higher uptake of the biological fluid), the measurement could be indicated by a phase lag of the oscillations. This phase lag becomes even more important when augmenting α_{th} in Figure 6. There, the incremental behaviour has completely vanished and only the phase lag is observable as an indication of biological fluid uptake.

Figures 4 to 6 show that, depending on the ratio of the thermal relaxation time and the thermal diffusion characteristic time, the detection of the biological fluid uptake can be monitored by two distinctive ways. If the thermal diffusion time is smaller for a certain relaxation time, the fluid uptake can be monitored by a gradient of the temperature response, whilst for larger thermal diffusion times the uptake can be followed by measuring the phase lag of an oscillatory temperature response. This can open ways to several types of biosensors.

5. Conclusions

In this work, a study on the response of an imposed temperature oscillation at high frequency is performed, using as material a porous carbon nanotube-silica nanocomposite. The purpose is to measure the uptake of biological fluids by noting that the temperature response can be altered by the thermal properties of the material, which depends also on the uptake of the biological fluids. For this study, a heat flux from Extended Thermodynamics has been employed, combined with an energy balance and an equation for the effective thermal conductivity. It is important to note that the evolution equation for the heat flux, although taken from developments from Extended Thermodynamics and neglecting thereby non-local effects [1], corresponds also to Cattaneo's equation for heat transport [18]. The model for the effective thermal conductivity has been satisfactorily validated against experiments of a porous CNT-SiO_2 nanocomposite. The experiments concern a procedure of self-assembled porous nanocomposite structures, of which the thermal conductivities have been measured.

Subsequently, the temperature response (induced by the imposed oscillatory temperature) is calculated using the heat transport equations. The ratio of the relaxation time and the thermal diffusion time is also varied in order to appreciate the effect the thickness of a material could have on the response. The uptake of the biological fluid has an influence on the effective thermal conductivity, which will change the temperature response. Although, for a final application, such methodology should be implemented in electrical circuits (implying indirectly induced temperature pulses), the source of the temperature pulses is not the subject of this study. Rather, it provides the mathematical and conceptual tools allowing such possible implementations. It appeared indeed that the uptake of biological fluid, simulated here by an increase of the volume fraction, alters clearly the temperature response, and this even in two distinct ways. It appeared that this response was of oscillatory nature with a phase lag when the thermal diffusion time was much lower than the relaxation time. On the other hand, when the thermal diffusion time was much higher than the relaxation time, the response was rather of exponential growing nature towards an asymptotic value.

Acknowledgements

Financial support from BelSPo is acknowledged.

Conflict of interest

All authors declare no conflicts of interest in this paper.

References

1. H. Machrafi and G. Lebon, Size and porosity effects on thermal conductivity of nanoporous material with an extension to nanoporous particles embedded in a host matrix, *Phys. Lett. A*, **379** (2015), 968–973.
2. V. Jean, S. Fumeron, K. Termentzidis, et al., Monte Carlo simulations of phonon transport in nanoporous silicon and germanium, *J. Appl. Phys.*, **115** (2014), 024304.
3. H. Machrafi, C. Minetti, V. Miskovic, et al., Self-assembly of carbon nanotube-based composites by means of evaporation-assisted depositions: Importance of drop-by-drop self-assembly on material properties, *Mat. Chem. Phys*., **218** (2018), 1–9.
4. L. J. Ke, G. Z. Gao, Y. Shen, et al., Encapsulation of aconitine in self-assembled licorice protein nanoparticles reduces the toxicity in vivo, *Nanosc. Res. Lett.*, **10** (2015), 449.
5. C. C. B. Bufon, J. D. C. González, D. J. Thurmer, et al., Self-assembled ultra-compact energy storage elements based on hybrid nanomembranes, *Nano Lett.*, **10** (2010), 2506–2510.
6. G. W. Hsieh, P. Beecher, F. M. Li, et al., Formation of composite organic thin film transistors with nanotubes and nanowires, *Physica E*, **40** (2008), 2406–2413.
7. J. Ding, X. Li, X. Wang, et al., Pressure-assisted self-assembly technique for fabricating composite membranes consisting of highly ordered selective laminate layers of amphiphilic graphene oxide, *Carbon*, **68** (2014), 670–677.
8. K. K. Rangharajan, K. J. Kwak, A. T. Conlisk, et al., Effect of surface modification on interfacial nanobubble morphology and contact line tension, *Soft Mat.*, **11** (2015), 5214–5223.
9. B. G. Prevo, D. M. Kuncicky and O. D. Velev, Engineered deposition of coatings from nano- and microparticles: A brief review of convective assembly at high volume fraction, *Coll. Surf. A: Physicochem. Eng. Asp.*, **311** (2007), 2–10.
10. R. Zhang, T. A. Elkhooly, Q. Huang, et al., A dual-layer macro/mesoporous structured TiO_2 surface improves the initial adhesion of osteoblast-like cells, *Mat. Sci. Eng. C*, **78** (2017), 443–451.
11. D. Wang, S. Liu, B. J. Trummer, et al., Carbohydrate microarrays for the recognition of cross reactive molecular markers of microbes and host cells, *Nat. Biotech.*, **20** (2002), 275–281.
12. I. I. Smalyukh, O. V. Zribi, J. C. Butler, et al., Structure and dynamics of liquid crystalline pattern formation in drying droplets of DNA, *Phys. Rev. Lett.*, **96** (2006), 177801.
13. H. Machrafi and G. Lebon, General constitutive equations of heat transport at small length scales and high frequencies with extension to mass and electrical charge transport, *Appl. Math. Lett.*, **52** (2016), 30–37.
14. H. Machrafi, An extended thermodynamic model for size-dependent thermoelectric properties at nanometric scales: Application to nanofilms, nanocomposites and thin nanocomposite films, *Appl. Math. Mod.*, **40** (2016), 2143–2160.

15. S. Sinha, S. Barjami, G. Iannacchione, et al., Off-axis thermal properties of carbon nanotube films, *J. Nanopart. Res*., **7** (2005), 651–657.
16. J. Hone, Phonons and thermal properties of carbon nanotubes, *Carbon Nanotubes. Topics in Applied Physics (eds M.S. Dresselhaus, G. Dresselhaus and P. Avouris)*, **80** (2001), 273–286.
17. Z. Y. Ong and E. Pop, Molecular dynamics simulation of thermal boundary conductance between carbon nanotubes and SiO_2, *Phys. Rev. B*, **81** (2010), 155408.
18. C. Cattaneo, Sulla conduzione del calore, *Atti Sem. Mat. Fis. Univ. Mod.*, **3** (1948), 83–101.

AIMS Press